SUPPLEMENTAL FIGURE LEGENDS

Supplemental Figure S1

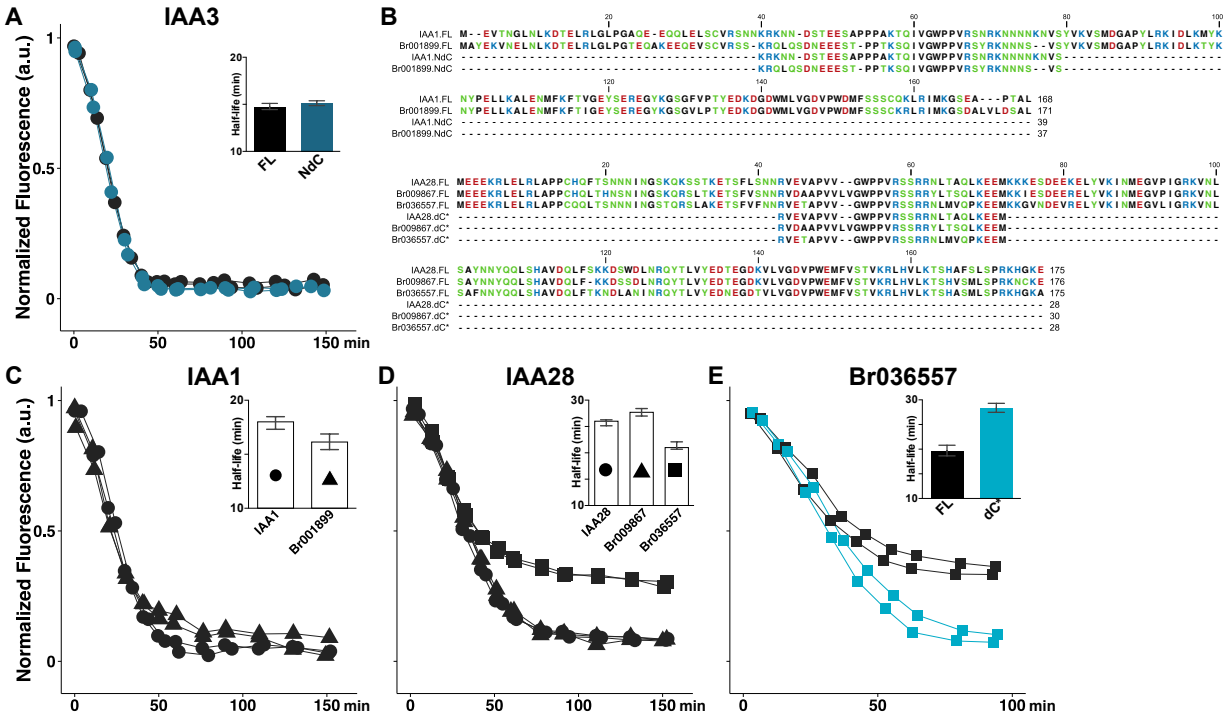

Supplemental Figure S1: Sequences flanking the degron are required to recapitulate degradation rates of full-length IAA3 and are conserved in *Brassica rapa* orthologs. A) A short peptide (NdC, blue) of *Arabidopsis thaliana* IAA3 is able to degrade at least as rapidly as the respective full-length (FL) protein (black) as assessed by time-lapse fluorescence flow cytometry. To facilitate comparison of degradation dynamics, mean fluorescence values were normalized to starting fluorescence. All data represent two independent experiments. Half-lives in this and all following panels represent means calculated from non-linear regression fits such as those as shown in Fig. 2B. Error bars represent 95% confidence intervals. **B)** Alignments of full-length, NdC and dC* fragments of *A. thaliana* IAA1 and IAA28 with their putative *B. rapa* orthologs. **C-D)** Full-length *B. rapa* IAA1 (C) and IAA28 (D) orthologs exhibit similar auxin-induced degradation dynamics as their *A. thaliana* counterparts when co-expressed with *A. thaliana TIR1* in yeast. **E)** The FL and dC* fragment of one putative *B. rapa* IAA28 ortholog (Br036557) exhibited different degradation dynamics.

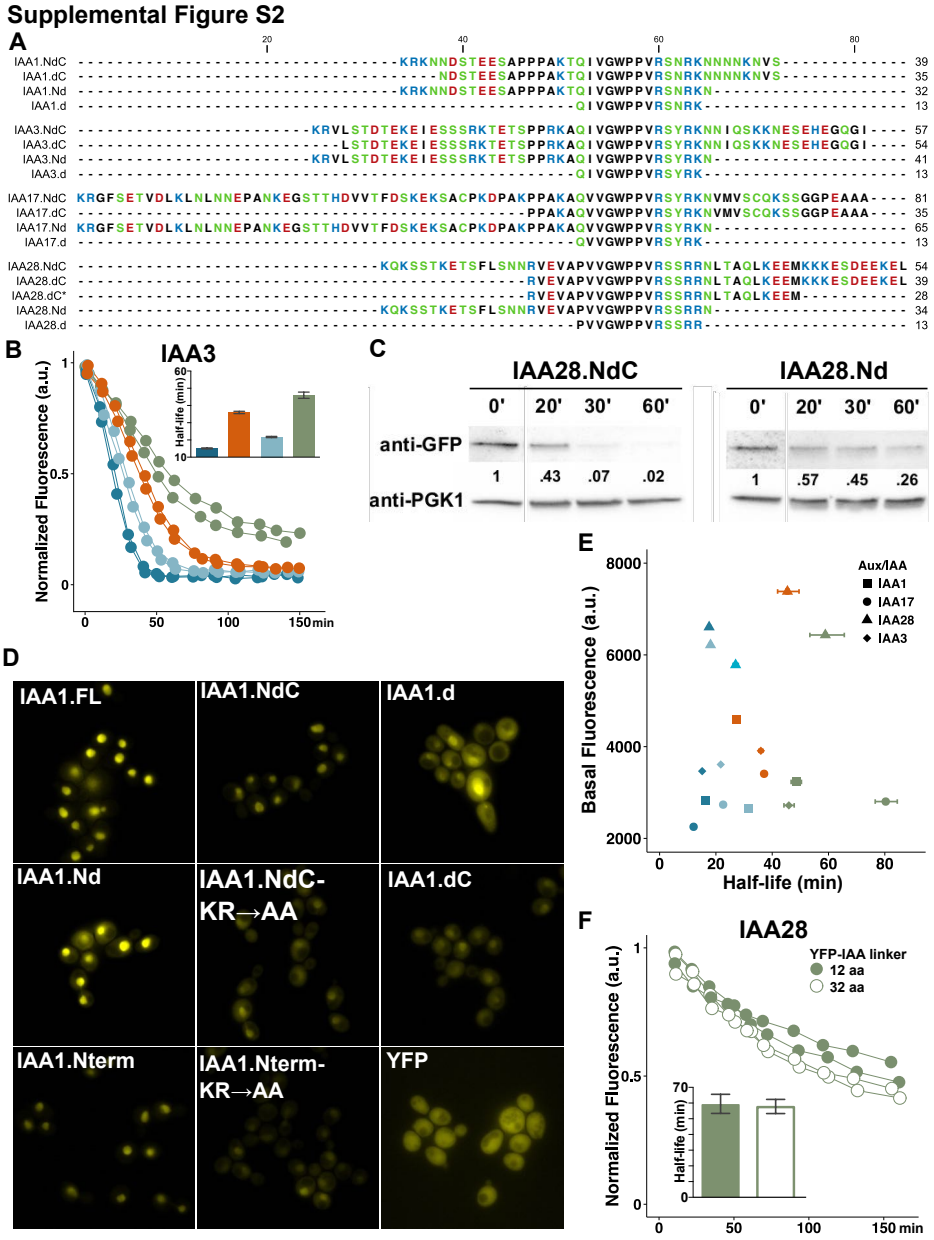

Supplemental Figure S2: The influence of N- and C-terminal rate motifs on degradation dynamics is IAA-dependent and is not confounded by differences in nuclear localization, basal expression, or linker length. A) Alignments of NdC, dC, dC*, Nd, and d fragments of IAA1, IAA3, IAA17, and IAA28. **B)** Regions N- and C-terminal of the degron influence IAA3 degradation dynamics. Colors in this and the following Supplemental Figures is consistent with Aux/IAA truncations indicated in Fig. 2A. Auxin-induced degradation in the presence of TIR1 was captured as before; half-lives in this panel (inset), and all subsequent panels, are presented with 95% confidence intervals. **C)** IAA28.NdC degrades faster than IAA28.Nd in yeast. Western

blot of auxin-induced IAA28.NdC and IAA28.Nd degradation in diploid yeast co-expressing TIR1 and the indicated YFP-IAA28 fragment. Whole cell lysates were prepared at various time points after treating with 10 μM auxin. **D)** All YFP-IAA1-2xSV40 fusion proteins localized in the nucleus of diploid yeast cells, though intensity differed between the constructs. **E)** Aux/IAA degradation rate did not correlate with levels of basal expression. Basal fluorescence intensity (e.g. pre-auxin treatment) of each YFP-IAA was plotted against the degradation half-life. These values were determined using nonlinear regression of the fluorescence degradation time courses obtained by flow cytometry (Fig. 2B-D, S2B). Error bars represent 95% confidence intervals. **F)** YFP-degron linker length did not contribute to degradation speed. IAA28.d fragments containing a 12 or 32 amino acids (aa) linker between the YFP moiety and the degron were co-expressed with TIR1 in yeast.

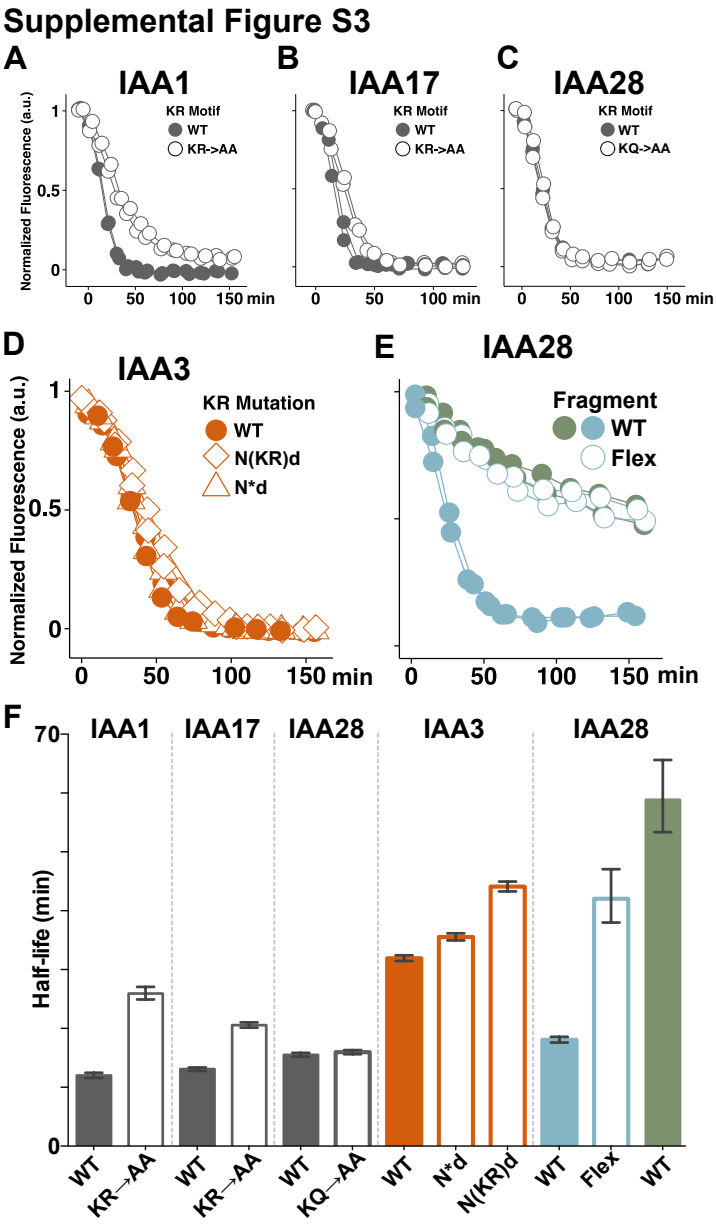

Supplemental Figure S3: The N-terminal KR residues contribute to Aux/IAA degradation rate, while rate determinants in the C-terminus cannot be replaced with a flexible linker. **A-C)** Mutating the KR rate motif in the context of the Nterm fragment slowed degradation of IAA1 (A) and IAA17 (B), but not IAA28 (C). **D)** Altering the KR-to-degron distance in IAA3 had no effect or slightly slowed IAA3.Nd degradation. **E)** Replacing the C-terminal rate motif of IAA28.dC with a flexible linker of identical length (4xGGSGG linker, IAAA28.dC-Flex) resulted in slower degradation dynamics than observed for the wild-type IAA28.dC fragment. **F)** Half-lives with 95% confidence intervals for data in A-E.

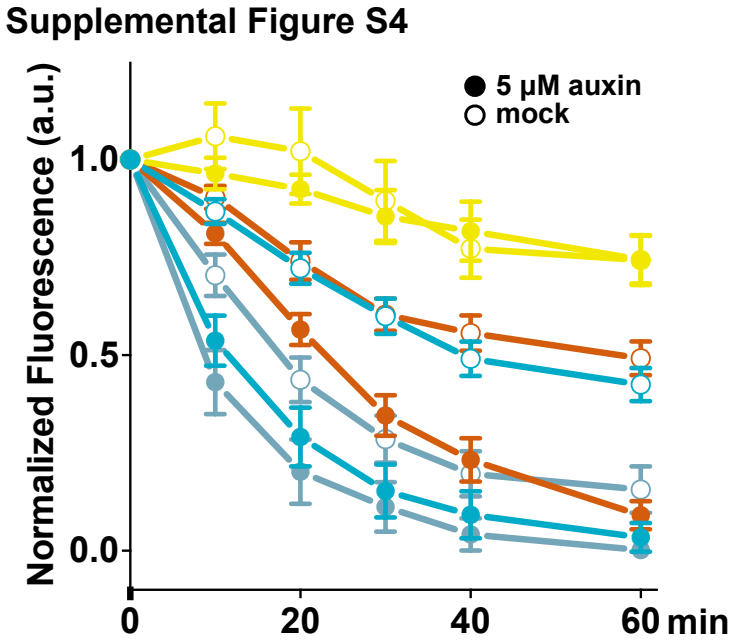

Supplemental Figure S4: Degradation of VENUS-IAA28 fragments in plant roots.
Auxin-induced VENUS-IAA28 degradation in *Arabidopsis* root tips. Data shown represent root tips treated with 5 µM exogenous auxin (closed symbols) or mock (95% ethanol, open symbols) and are normalized as shown in Fig. 4B. The IAA28 fragments are consistent with those described in Fig. 2A: light blue for IAA28.dC, bright blue for IAA28.dC*, orange for IAA28.Nd; yellow represents VENUS-alone.

Supplemental Figure S5

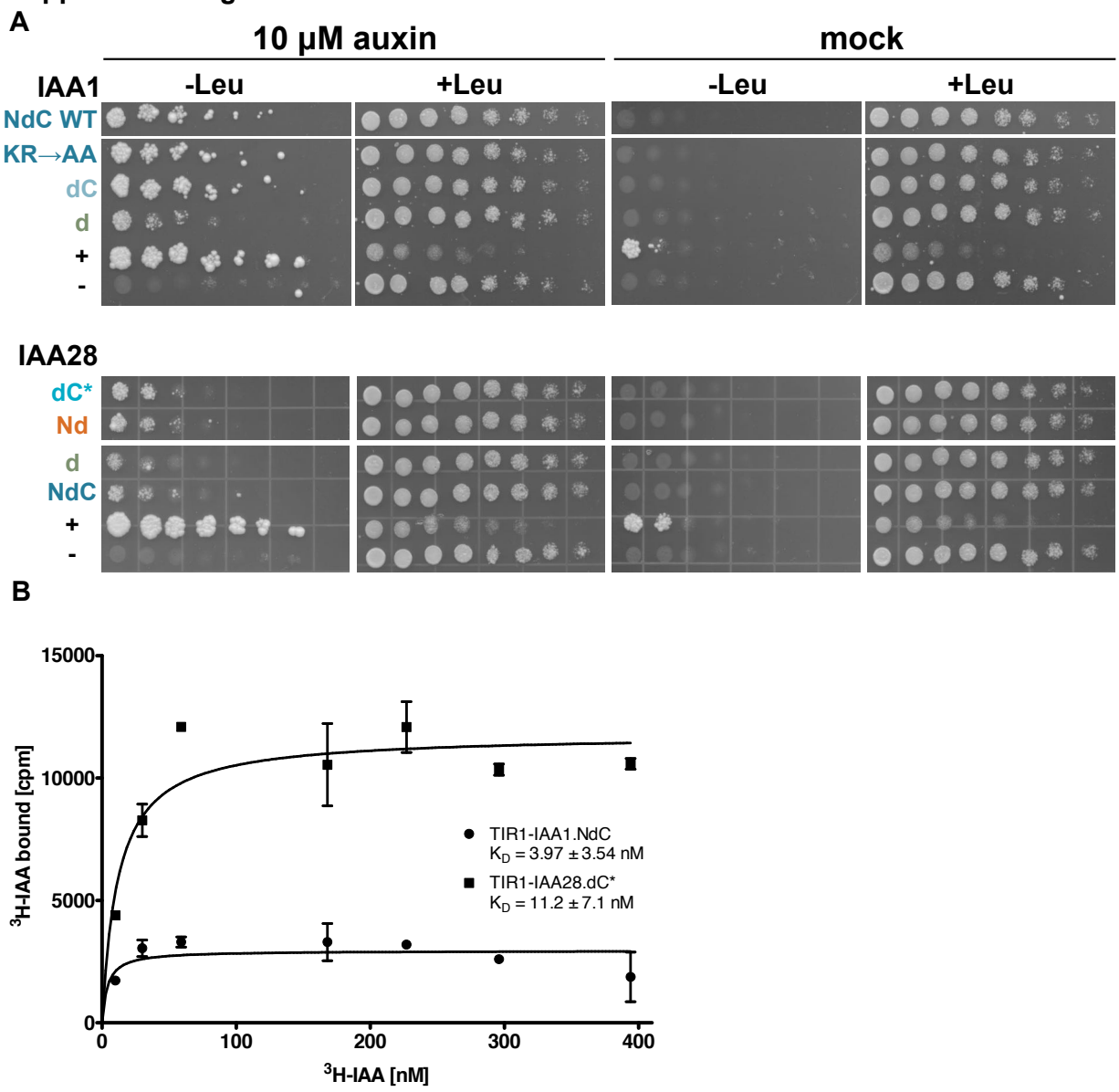

Supplemental Figure S5: Binding affinity between IAA28 and IAA1 fragments and the TIR1 auxin receptor is not always correlated with degradation rate. A) Interaction between TIR1 and several IAA1 and IAA28 peptides was assessed by yeast two hybrid assay in the presence of 10 µM auxin or mock (95% ethanol). Media lacking leucine selects for interaction, while media supplemented with leucine serves as a growth control. Technique control strains were yeast co-expressing full-length IAA7 (+) or empty vector (-) and TIR1. **B)** Radiolabeled auxin binding of TIR1 in complex with IAA1.NdC or IAA28.dC*.

SUPPLEMENTAL PROTOCOL S1: MATERIALS & METHODS

Saturation Auxin Binding Assays

Radioligand binding assays were performed as previously described in Calderón Villalobos *et al.* (2012). In brief, binding assays were carried out using highly pure recombinant TIR1-ASK1 protein complex and N-terminal GST-tagged AUX/IAA protein truncations. Duplicate samples containing proteins, radiolabeled indole-3-acetic acid (IAA) and cold competitor (unlabeled IAA) were incubated for one hour on ice, subsequently filter-immobilized, and washed with binding buffer. Filters were incubated overnight in scintillation buffer and retained radiolabeled auxin was measured via scintillation counting. Nonspecific binding was determined using a 10,000-fold excess of cold IAA with respect to [^{3}H]-IAA. Data analysis was performed using GraphPad Prism 5 software. K_D values were obtained applying one site binding (hyperbola) model. Specific binding was calculated as the difference of average total binding and nonspecific binding. Samples for total and non-specific binding were in duplicates.